ACS APPLIED MATERIALS & INTERFACES
RESEARCH ARTICLE
www.acsami.org

Magnetic Mesoporous Organic–Inorganic $NiCo_2O_4$ Hybrid Nanomaterials for Electrochemical Immunosensors

Qunfang Li,[†,‡] Lingxing Zeng,[†,§] Jinchao Wang,[§] Dianping Tang,[*,‡] Bingqian Liu,[‡] Guonan Chen,[‡] and Mingdeng Wei[*,§]

[‡]Key Laboratory of Analysis and Detection for Food Safety (Ministry of Education & Fujian Province), Department of Chemistry, Fuzhou University, Fuzhou 350108, China

[§]Institute of New Energy Technology and Nano-Materials, Fuzhou University, Fuzhou 350002, China

ABSTRACT:

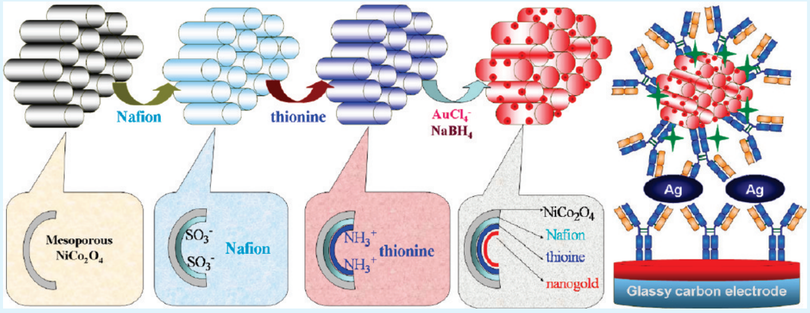

This study demonstrates a facile and feasible strategy toward the development of advanced electrochemical immunosensors based on chemically functionalized magnetic mesoporous organic–inorganic hybrid nanomaterials, and the preparation, characterization, and measurement of relevant properties of the immunosensor for detection of carcinoembryonic antigen (CEA, as a model analyte) in clinical immunoassays. The as-prepared nanomaterials composed of a magnetic mesoporous $NiCo_2O_4$ nanosheet, an interlayer of Nafion/thionine organic molecules and a nanogold layer show good adsorption properties for the attachment of horseradish peroxidase-labeled secondary *anti*-CEA antibody (HRP-*anti*-CEA). With a sandwich-type immunoassay format, the functional bionanomaterials present good analytical properties to facilitate and modulate the way it was integrated onto the electrochemical immunosensors, and allows the detection of CEA at a concentration as low as 0.5 pg/mL. Significantly, the immunosensor could be easily regenerated by only using an external magnet without the need of any dissociated reagents. Importantly, the as-synthesized magnetic mesoporous $NiCo_2O_4$ nanomaterials could be further extended for detection of other biomarkers or biocompounds.

KEYWORDS: magnetic organic–inorganic hybrid nanomaterials, mesoporous $NiCo_2O_4$ nanosheets, electrochemical immunosensor, carcinoembryonic antigen

INTRODUCTION

Developing the methodology of biomolecular recognition elements that reveal the reproducible improvement and sensitive enhancement is crucial in proteomics and clinical diagnostics.[1] In general, the assay is implemented by using certain affinity ligands, e.g., antibody and aptamers, which specifically react with the protein, and thus mediate a target-responsive signal-produced cascade.[2] Electrochemical immunosensors hold great potentials as the next-generation detection strategy due to their high sensitivity, low cost, ease of miniaturization, and so on.[3] For the successful development of an electrochemical immunosensor, signal amplification and noise reduction are very vital.[4] Typically, these properties strongly depend on the transducer and signal-produced protocol.[5] Although the label-free electrochemical measurements make a little requirement for operational steps and reagents, the detectable signal and sensitivity are usually limited. Ongoing effort has been made worldwide by using signal-produced labels as sensitive amplification, such as bioactive enzymes, metal nanoparticles, quantum dots, carbon nanotubes, and organic–inorganic nanomaterials with redox activity.[6−9]

Binary compounds (M_xO_y), especially magnetic nanomaterials, are of intense interests in biomaterial research because of their remarkable magnetic, electrical, optical and catalytic properties.[10] Among these nanomaterials, the cobalt-containing spinel oxides MCo_2O_4 (M = Cu, Mn, Ni, Zn, Mg, etc.) have drawn considerable attention by virtue of their superior physicochemical properties and tremendous potential for many technological applications, ranging from catalysts and sensors to electrode materials and electrochemical devices.[11] Mesoporous spinel cobaltites with large surface-to-volume ratios and uniform pore diameters are desirable especially for processes taking place at the phase boundary between solid particles and a liquid or gas phase as well as those relying on the flux of

Received: February 21, 2011
Accepted: March 30, 2011
Published: March 30, 2011

dx.doi.org/10.1021/am200228k | *ACS Appl. Mater. Interfaces* 2011, 3, 1366–1373

biomolecules or ions to and from active surfaces.[12] Therefore, the mesoporous nanomaterials with the unique magnetic properties not only act as an affinity support for the assembly of biomolecules, but also enable the rapid separation and purification of biomaterials after synthesis. However, most magnetic nanoparticles without modification are easily aggregated into clusters in the solution because of the magnetic dipolar attraction, which limits their utilization in the biological analysis. To overcome this shortcoming, variously functionalized magnetic nanomaterials have been synthesized and applied in the bioanalysis, e.g. superparamagnetic iron oxide with a hydrophobin PLGA core and a positively charged glycol chitosan shell,[13] magnetic core−core−shell Fe_3O_4−Prussian blue−gold nanostructures,[14] protein A-functionalized magnetic beads,[15] Recently, our group also synthesized various magnetic nanomaterials for the conjugation of biomolecules, such as magnetic-core/porous-shell CoFe2O4/SiO2 nanoscales,[16] core−shell $NiFe_2O_4/SiO_2$ composite nanoparticles,[17] thionine-doped magnetic gold nanospheres,[18] and Prussian blue-doped magnetic silica nanocomposites.[19] Following that, we also found that magnetic nanomaterial-labeled biomolecules exhibited relatively weaker conductivity in comparison with pure biomolecules. The reason might be the fact that most magnetic nanoparticles possess low conductivity, which might hinder the electron transfer.

In view of these consideration, use of magnetic mesoporous nanomaterials should be preferable as the following advantages: (i) The conductivity of magnetic porous nanomaterials can be improved by doping noble metallic nanoparticles into the pores with an in situ synthesized method (e.g., nanogold or nanosilver particles), and the penetrated nanoparticles can serve as an intervening "spacer" matrix for electron communication; (ii) magnetic mesoporous nanomaterials possess higher volume-to-surface ratio than that of solid nanoparticles, which can conjugate more biomolecules, and improve the sensitivity of bioanalysis. Gold nanoparticle, as a kind of well-know bionanomaterial, exhibits greatly chemical stability, large specific surface area, excellent electrical conductivity, excellent biocompatibility, strong adsorption ability, and well suitability.[20,21] The unique properties of nanogold-codified magnetic mesoporous nanomaterials coupled with the conjugation of biological components, provide a promising platform for the development of high-performance electrochemical immunosensors.

Herein, magnetic mesoporous $NiCo_2O_4$ nanosheets with three-dimension channels were initially synthesized, and then the organic−inorganic $NiCo_2O_4$ hybrid nanomaterials with a core−core−core−shell $NiCo_2O_4$−Nafion−thionine−nanogold format were fabricated on the magnetic mesoporous nanosheets. The as-prepared nanomaterials were utilized for the label of biomolecules by using horseradish peroxidase-conjugated carcinoembryonic antibody (HRP-*anti*-CEA) as a model, because CEA is an important tumor marker for colon cancer or gastrointestinal malignancies. We expected that use of magnetic mesoporous bionanomaterials could enhance the sensitivity and reproducibility of the electrochemical immunosensors. The aim of this study is to explore and exploit a novel bionanomaterial for the signal amplification of electrochemical immunosensor.

EXPERIMENTAL SECTION

Triblock copolymer of Pluronic (P123), Nafion (Nf, 5%, w/w) and thionine acetate salt (Th, Dye content ≥85%) were purchased from Sigma-Aldrich (St. Louis, MO, USA). Cobalt and nickel hydrous nitrates ($Co(NO_3)_2 \cdot 6H_2O$, $Ni(NO_3)_2 \cdot 6H_2O$), *n*-butylalcohol, HCl (37 wt%), $HAuCl_4 \cdot 4H_2O$, and tetraethoxysilane (TEOS) were purchased from Sinopharm Chem. Re. Co. Ltd. (Shanghai, China). Horseradish peroxidase-labeled *anti*-CEA antibody (HRP-*anti*-CEA, Ab_2), *anti*-CEA antibody (*anti*-CEA, Ab_1) and CEA standards were purchased from Biocell Biotech. Co. Ltd. (Zhengzhou, China). Bovine serum albumin (BSA, 96−99%) was purchased from Shanghai Medpep Co. Ltd. (Shanghai, China). All other reagents were of analytical grade and used without further purification. Deionized and distilled water was used throughout the study. 0.1 M acetic acid-buffered saline (ABS) with various pHs were prepared by mixing the stock solutions of 0.1 M HAc and 0.1 M NaAc, and 0.1 M KCl was added as the supporting electrolyte. 0.1 M phosphate-buffered saline (PBS, pH 7.4) was prepared by adding 12.2 g of K_2HPO_4, 1.36 g of KH_2PO_4, and 8.5 g of NaCl into 1000 mL of deionized water.

XRD patterns were recorded on a PANalytical X'Pert spectrometer using the Co Kα radiation ($\lambda = 1.789$ Å), and the data would be changed to Cu Kα data. The sizes of nanoparticles were estimated from transmission electron microscopy (TEM) (H-7650, Hitachi Instrument, Japan). N_2 adsorption−desorption analysis was measured on a Micromeritics ASAP 2000 instrument (Micromeritics, Norcross, GA, USA). Pore volumes were determined using the adsorbed volume at a relative pressure of 0.99. Multipoint Brunauer−Emmet−Teller (BET) surface area was estimated from the relative pressure range from 0.06 to 0.3. The pore size distributions of the as-prepared samples were analyzed using the Barrett−Joyner−Halenda (BJH) method. Magnetic measurements were made using Nanjing University Instruments on vibrating sample magnetometer (VSM) at room temperature that produces fields of up to 6 T on the sample. Fourier transform infrared spectroscopy (FT-IR) of the bionanomaterials was characterized by FT-IR system (Spectrum GX, PerkinElmer, USA). X-ray photoelectron spectroscopy (XPS) measurements were carried out using a VG Scientific ESCALAB 250 spectrometer with Al Kα X-ray (1486.6 eV). All voltammetric measurements were carried out with a CHI 620D Electrochemical Workstation (Shanghai CH Instruments Inc., China). A three-compartment electrochemical cell contained a platinum wire auxiliary electrode, a saturated calomel reference electrode (SCE) and the modified glassy carbon electrodes (GCE, 3 mm in diameter) as working electrode.

Mesoporous silica KIT-6 was prepared according to procedures reported elsewhere.[22] High crystalline mesoporous $NiCo_2O_4$ were successfully prepared through the nanocasting strategy, using KIT-6 silica as a hard template. The general procedure was carried out as follows: nickel(II) nitrate hexahydrate ($Ni(NO_3)_2 \cdot 6H_2O$) and cobalt(II) nitrate hexahydrate ($Co(NO_3)_2 \cdot 6H_2O$) (total mass: 1 g) with the molar ratio of 1:2 were dissolved in ethanol to form a hybrid solution. After stirring at room temperature for 1 h, 0.5 g of KIT-6 was added. The suspension was stirred until dry at room temperature and the sample then was calcined at 300 °C for 3 h. This procedure was repeated two times and then calcined at 380 °C for 4 h. The silica template was removed by etching twice with 2 M NaOH aqueous solution at 60 °C for 12 h each time. After centrifuging and decanting off the clear solution, the solid was washed thrice with distilled water and ethanol, and then dried at 80 °C to obtain the resultant $NiCo_2O_4$ replica.

The modification and bioconjugation of magnetic mesoporous $NiCo_2O_4$ nanosheets are schematically represented in Scheme 1, and described in detail as follows: (i) 3 mg of $NiCo_2O_4$ nanosheets was dispersed into 2 mL ethanol solution containing 500 μL Nafion (5%, w/w), and the mixture was adequately stirred for 4 h at room temperature (RT) to obtain Nafion-enclosed $NiCo_2O_4$ organic−inorganic hybrid nanomaterials; (ii) the purified Nafion−$NiCo_2O_4$ nanostructures by centrifugation for 10 min at 8000 g were redispersed into 2.5 mL of thionine aqueous solution (3 mM), and slightly stirred at 150 rpm for 1 h at RT to make the positively charged thionine molecules adsorb onto the surface of negatively charged thinione-$NiCo_2O_4$ nanomaterials; (iii) 5 mL of $HAuCl_4$ aqueous solution (1%, w/w) was added into the purified thionine-Naftion-$NiCo_2O_4$ as mentioned above, and incubated

Scheme 1. Fabrication Process and Schematic Illustration of the $NiCo_2O_4$−Nf−Th−Au Nanomaterials, And Measurement Protocol of the Electrochemical Immunosensor

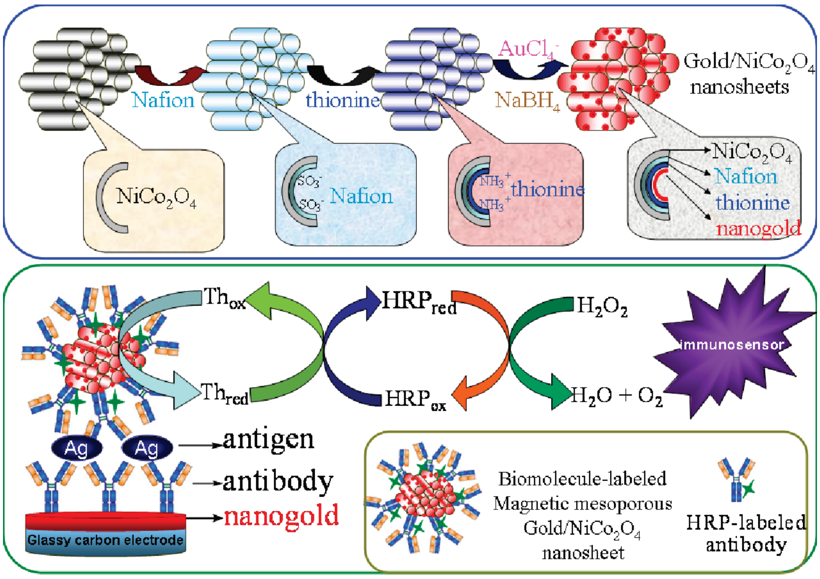

for 2 h at RT with slightly stirring in order to form $AuCl_4^-$ ions-functionalized magnetic mesoporous nanomaterials because of the strong interaction between the $AuCl_4^-$ ions and positively charged thionine molecules; and (iv) the Au(III) on/into the magnetic mesoporous nanomaterials was reduced to the zerovalent gold nanoparticles with the help of 0.1 mM $NaBH_4$ solution containing 0.3 mM NaOH. Finally, the formed organic−inorganic hybrid nanomaterials (denoted as $NiCo_2O_4$−Nf−Th−Au) were utilized for the label of HRP-*anti*-CEA secondary antibody.

The obtained $NiCo_2O_4$−Nf−Th-Au was initially dispersed into 2 mL pH 9.0 Tris-buffer solution, and then 500 μL of HRP-*anti*-CEA with original concentration was added into the solution. After incubated for 12 h at 4 °C with slightly stirring, the mixture was centrifuged for 10 min at 8,000 g. The obtained precipitation was added into 0.1 wt % BSA solution, and incubated for 1 h at RT to block possible remaining active sites of nanomaterials and avoid the nonspecific adsorption. The prepared bionanomaterials (denoted as $NiCo_2O_4$−Nf−Th−Au−Ab_2) were stored into pH 7.4 PBS at 4 °C until use.

Prior to electrochemical measurements, the immunosensor was fabricated according to our previous report with a little modification.[18] Briefly, a layer of nanogold particles was initially electrodeposited on the GCE surface by using a potential-step electrolysis from +1.1 to 0 V in 0.5 M H_2SO_4 solution containing 1.0 mM $HAuCl_4$ with different pulse times, i.e., 10, 30, and 60 s. Following that, the nanogold-modified GCE was immersed in the *anti*-CEA solution, and incubated for 12 h at 4 °C. Subsequently, the possible remaining active sites on the electrode were blocked by using 0.1 wt % BSA as the mentioned method above. The as-prepared immunosensor (denoted as Ab_1/AuNP/GCE) was used for detection of CEA analyte.

The electrochemical measurement of the immunosensor toward CEA samples or standards was carried out with a sandwich-type immunoassay mode by using $NiCo_2O_4$−Nf−Th-Au-Ab_2 as traces and H_2O_2 as enzyme substrates. The assay mainly consisted of three steps as follows: (i) the as-prepared immunosensor was incubated with various concentrations of CEA samples for 25 min at RT to form the antigen−antibody immunocomplex on the Ab_1/AuNP/GCE; (ii) the modified electrode was reincubated with the as-prepared bionanomaterials (i.e., $NiCo_2O_4$−Nf−Th−Au−Ab_2) for another 25 min at RT to construct a sandwiched immunocomplex on the Ab_1/AuNP/GCE; and (iii) the electrochemical behavior of the immunosensor was recorded into pH 5.5 ABS containing 6.0 mM H_2O_2 by differential pulse voltammetry (DPV) from 150 to −550 mV (vs. SCE) with a pulse amplitude of 50 mV and a pulse width of 20 ms. The DPV peak current was collected and registered as the signal of the immunosensor relative to the concentration of CEA sample.

RESULTS AND DISCUSSION

Figure 1A shows the wide-angle XRD pattern of $NiCo_2O_4$ synthesized using KIT-6 as a hard template. All the diffraction reflections can be indexed to a cubic spinel $NiCo_2O_4$ (JCPDS 073−1702), and no impurity phase was detected. The low-angle XRD pattern of KIT-6 silica and $NiCo_2O_4$ are depicted in Figure 1B. Figure 1B-a shows three well-defined peaks in the region $2\theta = 0.5-3°$ that can be indexed as (211), (220), and (420) Bragg reflections, indicating that KIT-6 has a highly ordered pore structure. As shown in Figure 1B-b, only single broaden reflection (211) was observed for mesoporous $NiCo_2O_4$, indicating that the synthesized mesoporous $NiCo_2O_4$ has a short-range ordered structure.[23]

Figure 2a shows the typical TEM image of magnetic mesoporous $NiCo_2O_4$ nanosheets. As seen from the inset of Figure 2a, magnetic mesoporous $NiCo_2O_4$ still retains a regular array of three-dimensional channels, and the frameworks are composed of high crystalline nanoparticles. Moreover, many small pores could be obviously observed. Moreover, the mesoporous nanostructures could be also observed after thionine and Nafion were immobilized on the surface of $NiCo_2O_4$ nanosheets (Figure 2b). As shown in Figure 2c, a large number of gold nanoparticles could be achieved on the $NiCo_2O_4$ nanosheets after the formation of the $NiCo_2O_4$−Nf−Th-Au. The appearance of gold nanoparticles provided a biocompatible interface and a good microenvironment for the conjugation of biomolecules. To further verify the formation of complex nanomaterials, the as-prepared $NiCo_2O_4$−Nf−Th−Au was characterized by using XPS spectroscopy. Figure 3a represents the Ni2p, Co2p, O1s,

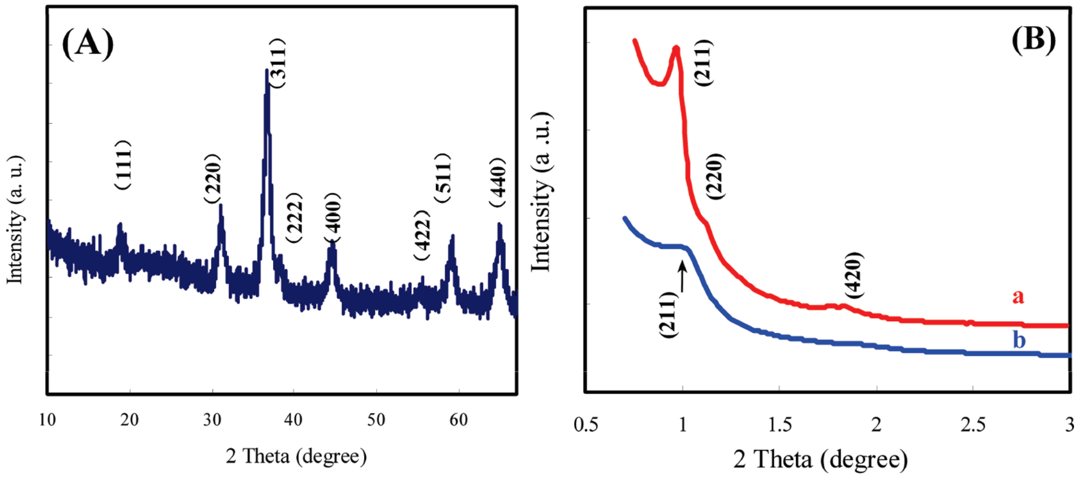

Figure 1. (A) Wide-angle XRD pattern of magnetic mesoporous $NiCo_2O_4$ nanosheets, (B) low-angle XRD patterns of (a) KIT-6 silica and (b) magnetic mesoporous $NiCo_2O_4$ nanosheets.

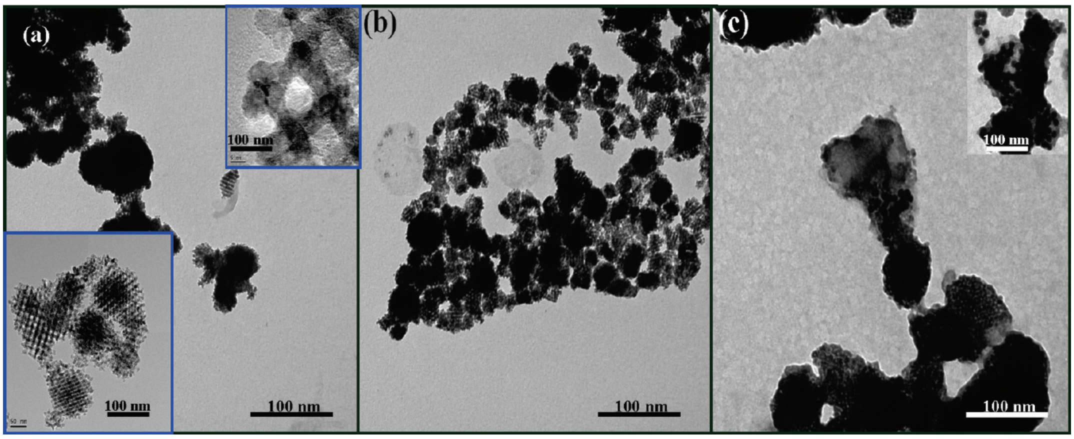

Figure 2. TEM images of (a) $NiCo_2O_4$ nanosheets (bottom inset, low-magnification image; top inset, high-magnification image), (b) $NiCo_2O_4$−Nf−Th, and (c) $NiCo_2O_4$−Nf−Th−Au nanomaterials (inset, magnification image).

N1s, C1s, S2p, and Au4f7 core level regions of the synthesized $NiCo_2O_4$−Nf−Th−Au nanomaterials, respectively. The existence of the new bands at 398.0 and 284.5 eV for $NiCo_2O_4$−Nf−Th indicated the presence of N1s and C1s. The inset of Figure 3a displays the XPS signature of the Au4f doublet (82.5 and 86.5 eV for the $4f_{7/2}$ and $4f_{5/2}$) for the resulting metallic Au^0. These results suggested that gold nanoparticles could be formed on the magnetic mesoporous nanosheets.

Next, type IV adsorption−desorption isotherms and H1 hysteresis loops of magnetic mesoporous $NiCo_2O_4$−Nf−Th−Au nanomaterials were investigated in the range of 0.7−1.0 Pa. The N_2 adsorption−desorption isotherm of magnetic mesoporous nanomaterials exhibits an isotherm of type IV isotherm (Figure 3b), corresponding to a characteristic of mesoporous materials. The pore size distribution of desorption branch is depicted in the inset of Figure 3b. It clearly shows a bimodal pore sizes distributions for mesoporous nanomaterials, which are common in KIT-6 type mesoporous materials.[24,25] The first peak at 3.3 nm can be attributed to the void space generated after the removal of silica wall, and is in good agreement with the pore size of mesoporous silica template KIT-6 silica, while a larger pore at 11.2 nm could be attributed to incomplete replicate in two sets of KIT-6 templates.[26] The specific surface area and larger pore volume of mesoporous $NiCo_2O_4$ are 122 $m^2\ g^{-1}$ and 0.42 $cm^3\ g^{-1}$, respectively. The high surface area and relatively large pores favored for the immobilization of biomolecules. Furthermore, magnetic property of $NiCo_2O_4$−Nf−Th−Au nanomaterials was also evaluated by using VSM method. As indicated from Figure 3c, the magnetization for the as-prepared $NiCo_2O_4$−Nf−Th−Au nanomaterials was 20.3 emu/g. So, the magnetization could still remain after modification.

To further monitor the interaction between $NiCo_2O_4$−Nf−Th−Au and biomolecules, we used the FT-IR spectrum. It is well-known that the shapes of the infrared absorption bands of amide I groups at 1610−1690 cm^{-1} corresponding to the C═O stretching vibration of peptide linkages and amide II groups around 1500−1600 cm^{-1} from a combination of N−H bending and C−N stretching can provide detailed information on the secondary structure of proteins.[27] The position of the amide I and II bands in the FTIR spectra of protein is a sensitive indicator of conformational changes in the protein secondary structure and has been used in the study to investigate the immobilized HRP-*anti*-CEA. As indicated from Figure 3d, the absorption bands for amide I and amide II bands in $NiCo_2O_4$−Nf−Th−Au−Ab_2 were located at 1648 and 1543 cm^{-1}, respectively. Therefore,

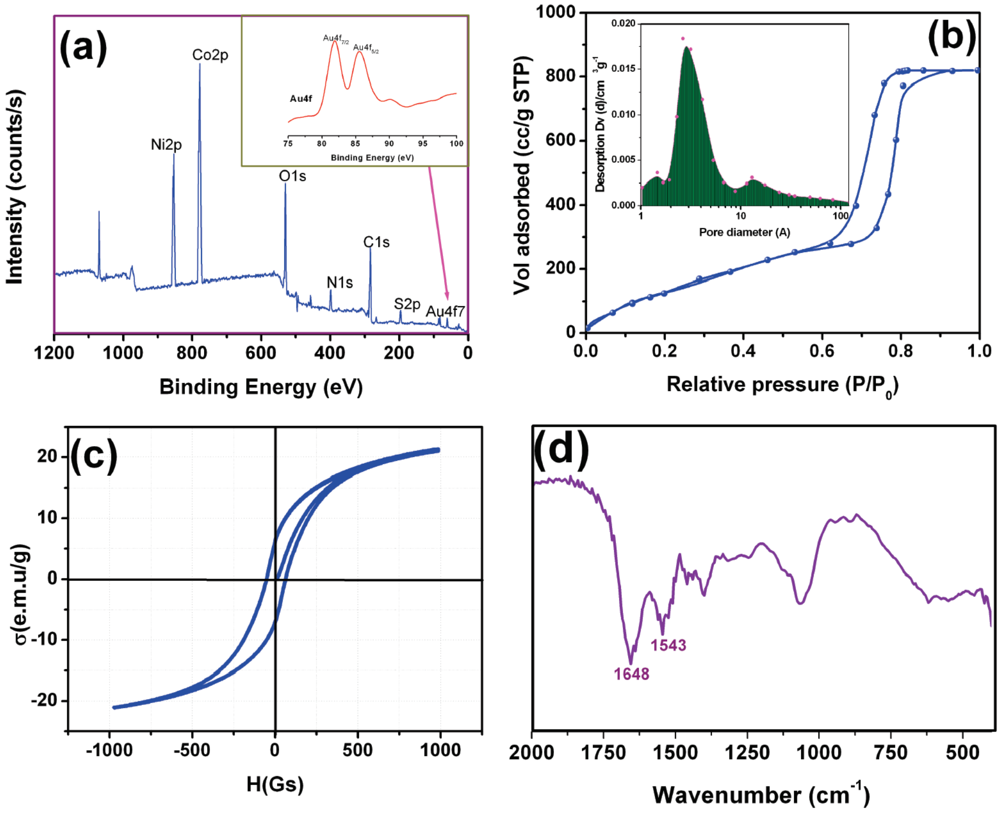

Figure 3. (a) XPS analysis (inset, Au4f core level spectra), (b) nitrogen adsorption—desorption isotherms (inset, pore size distribution), and (c) VSM analysis of NiCo$_2$O$_4$—Nf—Th—Au. (d) FT-IR spectroscopy of NiCo$_2$O$_4$—Nf—Th—Au—Ab$_2$.

the HRP-*anti*-CEA could be immobilized on the surface of NiCo$_2$O$_4$—Nf—Th—Au.

To monitor the possible application of the synthesized bionanomaterials in the bioanalysis, we used the as-prepared NiCo$_2$O$_4$—Nf—Th—Au—Ab$_2$ for detection of CEA (as a model analyte) in clinical immunoassays. Initially, the electrochemical behaviors and amplified properties of the immunosensor were investigated by using cyclic voltammetry (CV) and electrochemical impedance spectroscopy (EIS). Figure 4 shows the cyclic voltammograms of the immunosensor with various steps in pH 5.5 ABS without or with the enzyme substrate, H$_2$O$_2$. No redox peaks were observed at the Ab$_1$/AuNP/GCE (Figure 4a) before and (Figure 4b) after reaction with 50 ng/mL CEA in pH 5.5 ABS. The reason might be ascribed to the lack of redox substances and the weak conductivity of the antigen—antibody complex. When the resulting immunosensors were reacted with the NiCo$_2$O$_4$—Nf—Th—Au—-Ab$_2$, however, a couple of well-defined redox peaks at −108 and −159 mV was appeared at the working potential range in pH 5.5 ABS (Figure 4c). The redox waves mainly derived from the immobilized thionine molecules with redox activity on the NiCo$_2$O$_4$—NF—Th—Au—Ab$_2$. The results indicated that the synthesized NiCo$_2$O$_4$—NF—Th—Au—Ab$_2$ could preliminarily apply for the electrochemical immunosensors. Moreover, the peak separation ($\Delta E_p = E_{pa} - E_{pc}$) was about 50 mV. The good electrochemical behavior might be owing to the penetrated/coated gold nanoparticles into/onto the mesoporous nanomaterials. When 0.1 mM H$_2$O$_2$ substrate was added into pH 5.5 ABS, an obvious catalytic process with the decrease of anodic peak and the increase of cathodic peak was occurred at the sandwiched immunosensor (Figure 4d). Significantly, the cathodic currents increased with the increment of H$_2$O$_2$ concentration (Figure 4e). The catalytic reduction process relative to H$_2$O$_2$ suggested that the immobilized HRP biomolecules on the NiCo$_2$O$_4$—Nf—Th—Au could still maintain their natural bioactivity, and the synthesized NiCo$_2$O$_4$—Nf—Th—Au could effectively shuttle electrons from the base electrode surface to the redox center of the immobilized biomolecules.

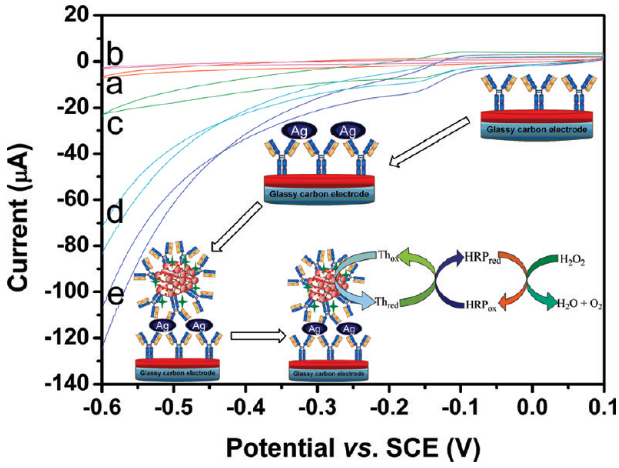

Figure 4. Cyclic voltammograms of (a) Ab$_1$/AuNP/GCE in pH 5.5 ABS, (b) the immunosensor *a* after reaction with 50 ng/mL CEA in pH 5.5 ABS, (c) the immunosensor *b* after reaction with NiCo$_2$O$_4$—Nf—Th—Au—Ab$_2$ in pH 5.5 ABS, and the immunosensor *c* in pH 5.5 ABS containing (d) 0.1 mM and (e) 6 mM H$_2$O$_2$ at 50 mV/s.

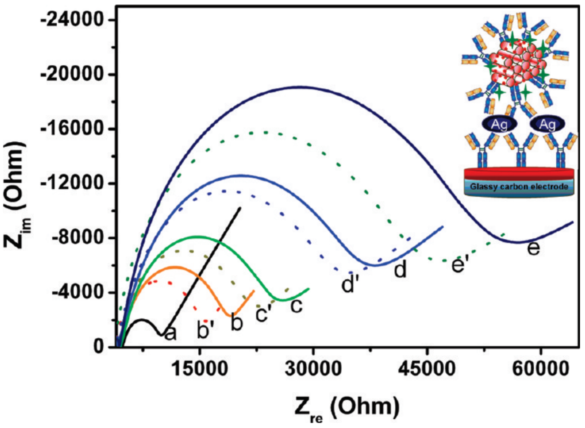

Figure 5. Electrochemical impedance spectroscopy of (a) Ab_1/AuNP/GCE, and the Ab_1/AuNP/GCE after incubation with (b) 1.0, (c) 10, (d) 30, and (e) 60 ng/mL CEA in pH 7.4 PBS containing 5 mM $Fe(CN)_6^{4-/3-}$ (Notes: Curves b′−e′ represent the EIS of the immunosensor b−e after incubation with excessive $NiCo_2O_4$−Nf−Th−Au−Ab_2, respectively).

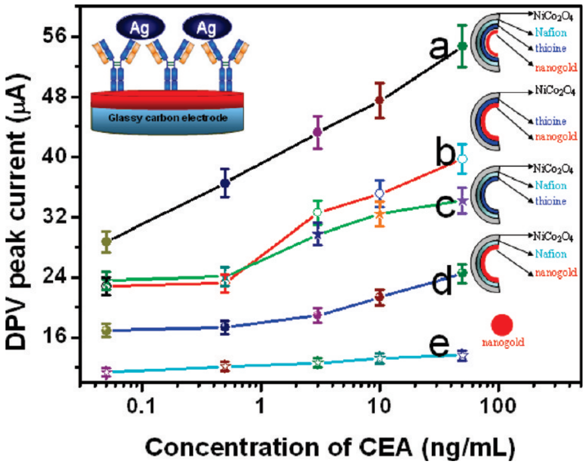

Figure 6. Electrochemical responses of the Ab_1/AuNP/GCE toward various concentrations of CEA samples by using (a) $NiCo_2O_4$−Nf−Th−Au−Ab_2, (b) $NiCo_2O_4$−Th−Au−Ab_2, (c) $NiCo_2O_4$−Nf−Th−Ab_2, (d) $NiCo_2O_4$−Nf−Au−Ab_2, and (e) Au−Ab_2 as signal antibodies.

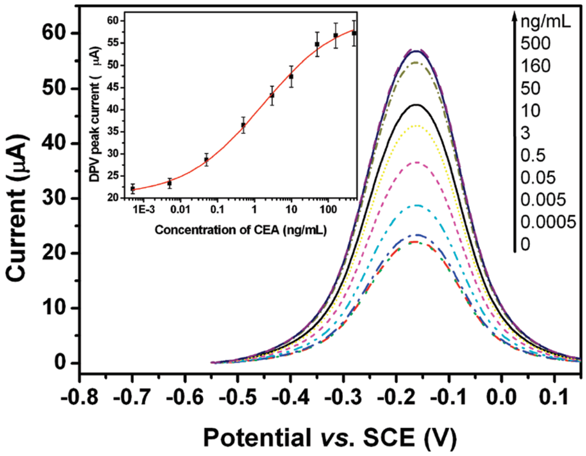

Figure 7. DPV curves of the electrochemical immunosensors toward various CEA standards by using $NiCo_2O_4$−Nf−Th−Au−Ab_2 in pH 5.5 ABS containing 6.0 mM H_2O_2 (inset, calibration curve) (Notes: incubation time, 25 min; incubation temperature, RT).

EIS can further give information on the impedance changes of the sensor interface in the modification process. It is well-known that the high frequency region of the impedance plots shows a semicircle related to the redox probe $Fe(CN)_6^{4-/3-}$, followed by a Warburg line in the low frequency region corresponding to the diffusion step of the overall process. The semicircle diameter of EIS equals the electron transfer resistance (R_{et}), which controls the electron transfer kinetics of the redox-probe at the electrode interface.[28] Figure 5a shows the typical Nyquist plots of the Ab_1/AuNP/GCE in 5 mM $Fe(CN)_6^{4-/3-}$ PBS (pH 7.4), and the resistance is 5160 Ω. The resistances gradually increased after the Ab_1/AuNP/GCE reacted with 1.0, 10, 30, and 60 ng/mL CEA (Figure 5b−e). The reason might be the fact that the formed immunocomplex between the antigens in the sample and the antibodies on the Ab_1/AuNP/GCE could serve as an inert layer, and hind the electron transfer. To further verify the merits of the synthesized bionanomaterials, we used the obtained electrodes in Figure 5b−e for further reaction with the $NiCo_2O_4$−Nf−Th−Au−Ab_2. As seen from Figure 5b′−e′, the resistances were decreased corresponding with those of curves b−e, respectively. The reason might be attributed to the fact that the synthesized $NiCo_2O_4$−Nf−Th−Au−Ab_2 possessed high conductivity and good electron transfer efficiency, which facilitate the electron communication between the solution and the base electrode.

In this contribution, the assay is based on a sandwich-type immunoassay format using $NiCo_2O_4$−Nf−Th−Au−Ab_2 as traces and H_2O_2 as enzyme substrates. To check up the amplification of the $NiCo_2O_4$−Nf−Th−Au−Ab_2 toward electrochemical signal, a comparative study of the electrochemical responses of the immunosensor was carried out on the Ab_1/AuNP/GCE by using variously labeled probes, such as $NiCo_2O_4$−Nf−Th−Au−-Ab_2, $NiCo_2O_4$−Th−Au−Ab_2, $NiCo_2O_4$−Nf−Th−Ab_2, $NiCo_2O_4$−Nf−Au−Ab_2, and Au−Ab_2. As seen from Figure 6, the immunosensor by using $NiCo_2O_4$−Nf−Th−Au−-Ab_2 exhibited higher sensitivity than those of other labeled probes. Some possible explanations might be considered as follows: (i) magnetic mesoporous $NiCo_2O_4$ nanoparticles could display a high surface-to-volume ratio, which could enhance the immobilized amount of biomolecules; (ii) Nafion, as a water-soluble polymer with negative charges, has excellent wetting properties and readily forms films in solution, which makes it as a coating or an additive to coatings; and (iii) thionine could be not only an excellent electron mediator, but also a good cross-linkage reagent between Nafion and nanogold.

Next, the $NiCo_2O_4$−Nf−Th−Au−Ab_2-based immunosensor was employed for detection of CEA standards as the mentioned above mode. Figure 7 shows the voltammograms of the $NiCo_2O_4$−Nf−Th−Au−Ab_2-based immunosensor toward various concentrations of CEA standards in pH 5.5 ABS containing 6 mM H_2O_2. A dramatic increase in the DPV peak currents was observed as the CEA concentration increased from 0.005 to 160 ng/mL. The detection limit (LOD, 3σ/S, in which σ is the standard deviation for the blank solution, $n = 13$, and S is the slope of the calibration curve) was 0.5 pg/mL. In contrast, the LOD of the magnetic mesoporous $NiCo_2O_4$-based immunosensor was lower 10 times than that of using magnetic solid $NiFe_2O_4$ nanoparticles previously reported by our group.[18] Moreover, the electrochemical immunosensor is also specific. To evaluate this property, we challenged the system with several other tumor

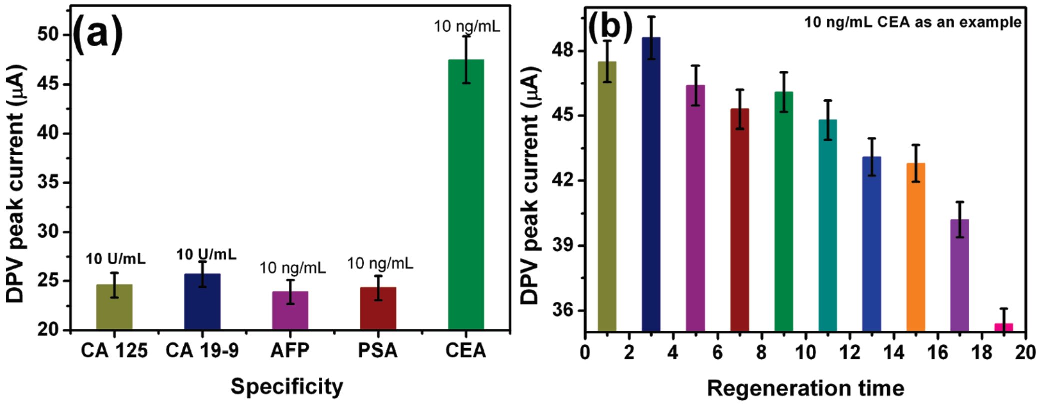

Figure 8. (a) Selectivity and (b) regeneration of the electrochemical immunosensor.

Table 1. Evaluation of Clinical Serum Specimen and Method Validation

	sample concentration (mean ± SD, ng/mL)[a]		
sample no.	by immunosensor	by ECL	RSD (%)
1	23.4 ± 1.1	25.3 ± 1.3	3.9
2	56.7 ± 2.7	49.5 ± 2.2	6.8
3	120.3 ± 4.6	132.1 ± 3.9	4.7
4	24.3 ± 2.4	26.4 ± 1.8	4.2
5	12.3 ± 0.9	13.4 ± 1.2	4.3
6	8.9 ± 0.7	7.8 ± 0.6	6.6
7	78.4 ± 3.2	72.1 ± 4.1	4.2
8	93.1 ± 3.7	97.3 ± 3.3	2.2
9	87.3 ± 5.6	93.1 ± 4.3	3.2
10	46.2 ± 1.4	42.3 ± 2.3	4.4
11	145.6 ± 6.7	136.7 ± 5.9	3.2
12	25.2 ± 1.6	24.2 ± 1.5	2.1
13	65.2 ± 3.1	59.8 ± 3.4	4.3
14	53.1 ± 2.8	58.3 ± 2.1	4.7

[a] The average value of three measurements.

markers: cancer antigen 125 (CA 125), cancer antigen 19−9 (CA 19−9), alpha-fetoprotein (AFP), and prostate-specific antigen (PSA). Significantly higher current response was observed with the target CEA than with other biomarkers (Figure 8a). These results clearly indicated the high specificity of the electrochemical immunosensor.

Regeneration of immunosensors is of interest to the immunoanalysts. Although the antibody−antigen linkage can be broken under drastic conditions (e.g., in alkalinic or acidic solutions or with chaotropic agents), the immobilized immunoreagents could also suffer from the functional damage or even be released from the immunosorbents. In this work, the immunosensor could be regenerated by simply using an external permanent $BaFe_{12}O_{19}$ magnet with block shape (55 × 14 × 10 mm, 410−430 mT) to remove the $NiCo_2O_4$−Nf−Th−Au−Ab_2−linked antigen.[14] Experimental results indicated that the immunosensor could keep 90.2% of the initial current response after regenerated for 15 times (Figure 8b). So, the immunosensor could provide a satisfactory reproducibility and regenerated performance. The stability of the electrochemical immunosensor was investigated. The immunosensor retained 90% of its initial current response after 21 days storage at 4 °C and decreased to 80% after 39 days.

Furthermore, the electrochemical immunosensor was further validated by assaying 14 clinical serum specimens, which were gifted from Fujian Provincial Hospital, China. The obtained results were compared with those of commercially available Electrochemiluminescent (ECL, Roche 2010, Switzerland) Analyzer as a reference method (Table 1). As shown in Table 1, the RSD was 0.1−28.1%. No significance differences were encountered, thereby revealing a good correlation between two methods.

To illustrate the generality of our design, we applied this strategy for the detection of staphylococcal enterotoxin B (SEB) in food by using *anti*-SEB/AuNP/GCE as the base electrode and HRP-*anti*-SEB-labeled Au−Th−Nf−$NiCo_2O_4$ as traces. Experimental results indicated that the $NiCo_2O_4$−Nf−Th−Au-based immunosensor could display a relatively low LOD of 0.1 pg/mL SEB (data not shown), which is 100-fold lower than that of the enzyme-nanosilica-doped carbon nanotube-based strategy previously reported by our group.[29]

■ CONCLUSIONS

In summary, this manuscript describes a simple and highly sensitive amplified electrochemical immunosensor by using magnetic mesoporous organic−inorganic hybrid $NiCo_2O_4$ nanomaterials with three-dimension channel for the first time. Compared with other labeled probes or magnetic solid nanostructures, the mesoporous nanoscales-based immunosensor could exhibit high sensitivity and low LOD. Highlight of this study is to make a highly conductive magnetic mesoporous nanomaterial for the amplification of the conventional sandwich-type electrochemical immunoassay. Although the as-prepared biomaterials are focused on the detection of the target CEA, it can be easily extend to the detection of other biomarkers in biological fluids or mycotoxins in foodstuff.

■ AUTHOR INFORMATION

Corresponding Author

*Tel./Fax: +86 591 22866125 (D.T.); +86 591 83753180 (M.W.). E-mail: dianping.tang@fzu.edu.cn (D.T.); wei-mingdeng@fzu.edu.cn (M.W.).

Author Contributions

†Q.L. and L.Z. contributed equally to this work.

■ ACKNOWLEDGMENT

Support by the National Natural Science Foundation of China (21075019, 20735002, 21073039), the Research Fund for the Doctoral Program of Higher Education of China

(20103514120003), the Award Program for Minjiang Scholar Professorship for Returned High-Level Overseas Chinese Scholars (XRC-0929), and the "973" National Basic Research Program of China (2010CB732403) is gratefully acknowledged.

REFERENCES

(1) Naesens, M. *Nat. Rev. Nephrol.* **2010**, *6*, 614–628.
(2) Brennan, D.; O'Connor, D.; Rexhepaj, E.; Ponten, F.; Gallagher, W. *Nat. Rev. Cancer* **2010**, *10*, 650–667.
(3) Pumera, M. *Chem. Soc. Rev.* **2010**, *39*, 4146–4157.
(4) Bard, A.; Zhou, H.; Kwon, S. *Israel J. Chem.* **2010**, *50*, 267–276.
(5) Williams, D. *Biomaterials* **2008**, *29*, 2941–2953.
(6) Williams, D. *Biomaterials* **2009**, *30*, 5897–5909.
(7) Williams, D. *Biomaterials* **2008**, *29*, 4037–4038.
(8) Rabaey, K.; Rozendal, R. *Nat. Rev. Microbiol.* **2010**, *8*, 706–716.
(9) Heinze, J.; Frontana-Uribe, B.; Ludwigs, S. *Chem. Rev.* **2010**, *110*, 4724–4771.
(10) Chen, F.; Shen, J.; Peng, B.; Pan, Y.; Tao, Z.; Chen, J. *Nat. Chem.* **2011**, *3*, 79–84.
(11) Zhang, G.; Guo, B.; Chen, J. *Sens. Actuator, B* **2006**, *114*, 402–409.
(12) Zhu, J.; Gao, Q. *Microporous Mesoporous Mater.* **2009**, *124*, 144–152.
(13) Lee, P.; Hsu, S.; Wang, J.; Tsai, J.; Lin, K.; Wey, S.; Chen, F.; Lai, C.; Yen, T.; Yen, T.; Sung, H. *Biomaterials* **2010**, *31*, 1316–1324.
(14) Zhuo, Y.; Yuan, P.; Yuan, R.; Chai, Y.; Hong, C. *Biomaterials* **2009**, *30*, 2284–2290.
(15) Eguilaz, M.; Moreno-Guzman, M.; Campuzano, S.; Gonzalez-Cortes, A.; Yanez-Sedeno, P.; Pingarron, J. *Biosens. Bioelectron.* **2010**, *26*, 517–522.
(16) Tang, D.; Yuan, R.; Chai, Y. *Adv. Funct. Mater.* **2007**, *17*, 976–982.
(17) Tang, D.; Yuan, R.; Chai, Y. *Clin. Chem.* **2007**, *53*, 1323–1329.
(18) Tang, D.; Yuan, R.; Chai, Y. *Anal. Chem.* **2008**, *80*, 1582–1588.
(19) Tang, D.; Su, B.; Tang, J.; Ren, J.; Chen, G. *Anal. Chem.* **2010**, *82*, 1527–1534.
(20) Park, B.; Yoon, D.; Kim, D. *Biosens. Bioelectron.* **2010**, *26*, 1–10.
(21) Parker, J.; Fields-Zinna, C.; Murray, R. *Acc. Chem. Res.* **2010**, *43*, 1289–1296.
(22) Cabo, M.; Pellicer, E.; Rossinyol, E.; Castell, O.; Surinach, S.; Baro, M. *Cryst. Growth Des.* **2009**, *9*, 4814–4821.
(23) Yang, P.; Zhao, D.; Margolese, D.; Chmelka, B.; Stucky, G. *Nature* **1998**, *396*, 152–155.
(24) Jiao, K.; Zhang, B.; Yue, B.; Ren, Y.; Liu, S.; Yan, S.; Dickinson, C.; Zhou, W.; He, H. *Chem. Commun.* **2005**, *45*, 5618–5620.
(25) Ren, Y.; Armstrong, A.; Jiao, F.; Bruce, P. *J. Am. Chem. Soc.* **2010**, *132*, 996–997.
(26) Jiao, F.; Hill, A.; Harrison, A.; Berko, A.; Chadwick, A.; Bruce, P. *J. Am. Chem. Soc.* **2008**, *130*, 5262–5266.
(27) Flach, C.; Cai, P.; Mendelsohn, R. *Adv. Technol. Biophys.* **2006**, *10*, 49–71.
(28) Prodromidis, M. *Electrochim. Acta* **2010**, *55*, 4227–4233.
(29) Tang, D.; Tang, J.; Su, B.; Chen, G. *J. Agric. Food Chem.* **2010**, *58*, 10824–10830.